Contrib Mineral Petrol (1991) 108:93–105

Contributions to Mineralogy and Petrology

Petrogenetic grids for metacarbonate rocks: pressure-temperature phase-diagram projection for mixed-volatile systems

James A.D. Connolly and Volkmar Trommsdorff

Institute für Mineralogie und Petrographie, Eidgenossische Technische Hochschule, CH-8092 Zürich, Switzerland

Received November 3, 1990 / Accepted January 21, 1991

Abstract. Isothermal or isobaric phase diagram sections as a function of fluid composition (X^F) are widely used for interpreting the genetic history of metacarbonate rocks. This approach has the disadvantages that: (1) the influence of a key metamorphic variable, either pressure (P) or temperature (T), is obscured; (2) the diagrams are inappropriate for systems that are not fluid-saturated. These problems are avoided by constructing phase-diagram projections in which the volatile composition of the system is projected onto a $P-T$ coordinate frame, i.e., a petrogenetic grid. The univariant curves of such $P-T$ projections trace the conditions of the invariant points of isothermal or isobaric phase-diagram sections, thereby defining the absolute stability of high-variance mineral assemblages, with and without a coexistent fluid phase. Petrogenetic grids for metacarbonate rocks are most useful for the study of regional metamorphism and for systems in which fluid composition has not been externally controlled. A calculated example of a $P-T$ projection for the system $CaO-MgO-SiO_2-H_2O-CO_2$ suggests that many assemblages (e.g., calcite + talc, enstatite + fluid, magnesite + tremolite, antigorite + diopside + dolomite, and calcite + forsterite + tremolite) in mixed-volatile systems have stability fields that make them useful as $P-T$ indicators. Consideration of the principles governing projection topology demonstrates that the univariant curves around a fluid present invariant point cannot be oriented independently with respect to the direction of compositional variation in the fluid phase. This has the interesting predictive implication that if the direction of compositional variation along one univariant curve around an invariant point is known, then the direction of compositional variation along the remaining curves can be determined solely from topologic constraints. The same constraints can be applied to systems containing simple mineral solutions or melts in order to predict compositional variations.

Offprint requests to: J.A.D. Connolly

Introduction

Phase diagrams and phase-diagram projections are a means by which the phase relations of a geologic system can be represented as a function of those properties of the system which cannot be directly measured. Generally, these are environmental properties such as pressure and temperature, but for systems in which a mixed-volatile fluid is a possible phase the composition of the fluid is also such a critical property. The importance of fluid composition as a geologic variable has been recognized since the classic work of Wyllie (1962) and Greenwood (1962), which has led to the widespread use of $T-X^F$ phase-diagram sections [1] (see Table 1 for notation). Such $T-X^F$ diagrams have proven valuable for many geologic applications, but they have limitations. The most significant of these is that pressure (or temperature in $P-X^F$ diagrams) is lost as an independent variable; thus, it is difficult to identify critical mineral assemblages in $T-X^F$ representations. Further, $T-X^F$ diagrams only show fluid-saturated phase relations, but fluid may be absent during stages in the evolution of a geologic system. This paper discusses an alternative representation in which fluid phase components are treated as true thermodynamic components (Connolly 1990) and the resulting phase diagram is projected onto the $P-T$ coordinate frame. The projected diagram, which is a petrogenetic grid, has the advantage that it clearly the $P-T$ fields of mineral assemblages in mixed-volatile systems. In addition, most of the compositional information shown in $T-X^F$ diagrams is retained in $P-T$ projections.

The construction and interpretation of phase-diagram projections for a system containing a fluid phase of variable composition requires only the principles originally formulated by Schreinemakers (1916, 1917, 1924; Zen 1966). However, because some of the features in such projections may be unfamiliar, and the relation of these

[1] $T-X^F$ diagrams are actually projections of a phase-diagram section, for brevity they will be referred to here simply as sections.

Table 1. Notation

Symbol	Meaning
c	Number of thermodynamic components
G	Gibbs free-energy function
P	Pressure, subscripted to indicate a particular condition
T	Temperature, subscripted to indicate a particular condition
X_j^i	Composition of phase i with respect to component j
α_i	Reaction coefficient of phase i
ν_i	Absolute value of α_i
ϕ_i	Composition vector of phase i

Symbol	Phase	Chemical composition
At	Antigorite	$Mg_{48}Si_{34}O_{85}(OH)_{62}$
C	CO_2-fluid	CO_2
Cc	Calcite	$CaCO_3$
Di	Diopside	$CaMgSi_2O_6$
Do	Dolomite	$CaMg(CO_3)_2$
E	Enstatite	$MgSiO_3$
Fo	Forsterite	Mg_2SiO_4
F	Fluid, unspecified composition	
F(x)	H_2O-CO_2 fluid, x is the mol% CO_2	
M	Magnesite	$MgCO_3$
Q	Quartz	SiO_2
Tc	Talc	$Mg_3Si_4O_{10}(OH)_2$
Tr	Tremolite	$Ca_2Mg_5Si_8O_{22}(OH)_2$
W	H_2O-fluid	H_2O

features to the more conventional $T-X^F$ projection may be unclear, the first part of this paper discusses a simple hypothetical system. The second part then presents a geologically relevant example. Although the utility of $P-T$ projections for mixed-volatile systems has been recognized for some time (Trommsdorff and Evans 1977a; Evans and Guggenheim 1988), calculation of the projections has been so tedious as to make them impractical. The appendix of this paper describes a method by which these calculations can be done efficiently by computer.

D.M. Carmichael (accepted for publication) has written a paper which parallels and in many ways compliments this contribution. The present paper differs substantially from Carmichael's in computational approach and in that more attention is devoted here to the theoretical basis of $P-T$ projections.

Phase diagram projections for a system with an H_2O-CO_2 fluid

To illustrate the features of $P-T$ projections for mixed-volatile systems consider the three component system $A-H_2O-CO_2$ containing five phases as shown in Fig. 1a. In this system, phases 3 and 4 are hydrocarbonate compounds, phases 1 and 2 are, respectively, hydrate and carbonate compounds, and the fifth phase, F, is an H_2O-CO_2 fluid. For purposes of illustration it is assumed that all compositions of this fluid are always stable. All five phases of the system can only be stable

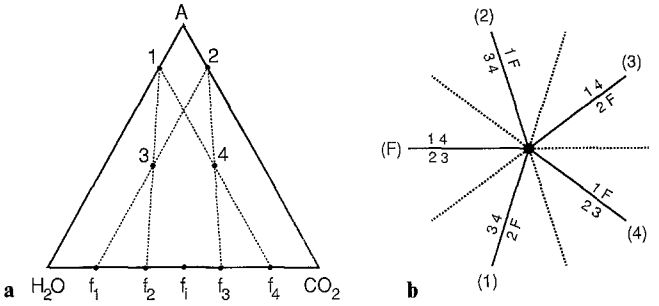

Fig. 1. a Chemographic relations among four compound phases (1–4) and an H_2O-CO_2 fluid in the hypothetical system $A-H_2O-CO_2$ as discussed in the text. Fluid compositions f_1–f_5 are singular compositions of the fluid which arise because of linear compositional degeneracies between the fluid and two compounds, as shown by the *dashed lines*. **b** Schreinemakers projection onto $P-T$ space of the univariant curves about an invariant condition at fluid composition f_i. Univariant curves are labeled by the corresponding reaction equations and, in parentheses, by the phases present at the invariant condition, but absent from the univariant equilibrium. Stable and metastable curves are drawn by *solid* and *dashed lines*, respectively

simultaneously at an invariant $P-T$ condition and at this condition the composition of the fluid coexisting with the other four phases is fixed, for example at composition f_i in Fig. 1a. Given this composition, the order of the five univariant curves (1), (F), (2), (3), and (4)[2] about the invariant $P-T$ point can be deduced, by Schreinemakers method, to be that shown in Fig. 1b (Zen 1966). The $P-T$ loci of each curve correspond to the equilibrium conditions of a chemical reaction defined by a mass-balance equation of the form:

$$0=\sum_{i=1}^{c+1} \alpha_i \phi_i \qquad (1)$$

where i indexes the phases in equilibrium, c is the number of thermodynamic components (Connolly 1990) for the system, ϕ_i is a vector describing the composition of the i^{th} phase, and α_i is the reaction coefficient of that phase. Following conventional usage, in the remainder of this paper the composition vector of any phase will be designated by the name of the phase.

Singular curves in $P-T$ projection

Of the five univariant curves in Fig. 1b, the reaction equation of (F) must have constant stoichiometric coefficients because the composition vectors of phases 1–4 are fixed. More generally, the composition of the fluid phase will vary continuously in each univariant equilibrium as a function of pressure and temperature; thus, the stoichiometric coefficients in the reaction equations of (1), (2), (3), and (4) must also vary continuously. In the

[2] Phase elements are identified here by listing in parentheses those phases which are possible in the system, but absent from the element, e.g., (1) denotes the phase element in which phases 2, 3, 4 and F coexist (Zen 1966).

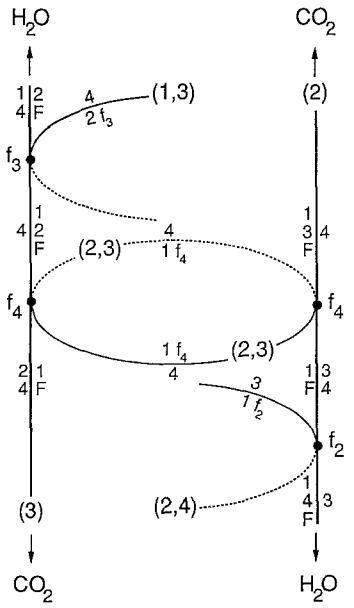

Fig. 2. Topology of singular points along univariant curves (2) (*right*) and (3) (*left*), for the system illustrated in **Fig. 1a**, as the fluid in each equilibrium varies from CO_2 to H_2O. Singular curves are drawn *thin*, and *dashed* if metastable. Singular points are labeled by the fluid phase composition (see **Fig. 1a**). The absolute stability of the non-degenerate curves is arbitrary, but the relative stabilities and topology of the curves are fixed, as discussed in the text. Note that if the univariant curves were drawn with different levels of stability, the (2, 3) singular curve would not close, except in connection with enantiomorphic singular points

course of such variation, the fluid may attain a composition such that the coefficient of one phase vanishes, such a composition is known as a *singular composition*. From Figs. 1a and 2, it can be seen that this occurs at fluid composition f_4 in the reaction equations of both (2) and (3). At this singular composition, the reaction equation for both (2) and (3) becomes $\nu_4\, 4 - \nu_1\, 1 - \nu_{f_4} f_4 = 0$ where $\nu_i = |\alpha_i|$. The equilibrium of this reaction defines an additional univariant curve, (2, 3), which degenerates with (2) and (3) when the composition of the fluid for these curves reaches f_4. The conditions at which this occurs are called *singular conditions* or *points*, and the univariant curve (2, 3) is called a *singular curve* to distinguish it from a curve corresponding to a non-degenerate equilibrium (Schreinemakers 1924). The composition of the fluid is fixed along a singular curve, thus the reaction equation for the equilibrium has constant coefficients, unlike the reaction equations of the non-degenerate univariant equilibria involving a fluid. For the phase compositions illustrated in Fig. 1a, there are three additional singular curves, (1, 4), (2, 4), and (1, 3), which occur at the fluid compositions, f_1, f_2, and f_3. Assuming that fluid composition in non-degenerate univariant equilibria changes monotonically with pressure and temperature[3], each singular curve will be tangent to two univariant curves at singular points. On either side of these points, the reaction coefficient of the phase present in the non-degenerate equilibrium, but absent from the singular element, must change sign.

There are several constraints on the relationship of a singular and non-degenerate univariant curve which become tangent at a singular point, these can be summarized by four rules, which may be deduced from Schreinemakers' discussion (1916):

(i) A singular curve cannot cross a univariant curve that represents an equilibrium which includes all the phases of the singular equilibrium (e.g., singular curve (2, 3) cannot cross either (2) or (3) in Fig. 2).

(ii) The stability of a non-degenerate univariant curve is not effected by a singular point.

(iii) On one side of a singular point, the non-degenerate univariant curve divides $P-T$ space into regions in which an assemblage (or phase), that includes neither the fluid nor the phases absent from the singular curve, is relatively more and less stable (e.g., phase 4 for both (2) and (3) at the f_4 singular points, Fig. 2). The singular equilibrium must occur in that region in which this assemblage is less stable.

(iv) The stability of the assemblage mentioned in (iii) is limited by the non-degenerate univariant curve on one side of the singular point. On the opposite side of the singular point, the singular curve must have the same level of stability as the non-degenerate univariant curve. The other extension of the singular curve must have a lower level of stability (e.g., in Fig. 2 the stability of phase 4 is limited by the reaction equations of both (2) and (3) on one side of the f_4 singular points, and (2, 3) is stable on the opposite side).

The above rules determine the topology of the singular and univariant curves about a singular point. A geologically relevant exception to rule 4, occurs when the singular fluid composition is extreme, i.e. pure H_2O or CO_2. In this case, the stability of the singular curve is not affected at the singular point, and on one side of the singular point both the univariant and singular curves coincide. At such a singular point, the singular curve may be relatively more stable than the univariant curve, but it cannot be less stable.

Arrangement of singular points about an invariant point

The relative stability of singular curves about a singular point is uniquely determined by Schreinemakers prinicples. This has the interesting implication that the direction in which the fluid composition changes along each univariant curve emanating from an invariant point cannot be independently specified in most cases. In general, it is possible, if not necessary, to draw the univariant curves around an invariant point with indifferent crossings, this can affect both the arrangement and stability of the singular points. The degree to which such a topology is constrained is determined by the number of singular equilibria that may occur in the system. This is a subject of considerable interest, but a digression in the context of this paper, and will be pursued further in

[3] This assumption implies that immiscibility does not occur in the fluid phase; therefore, the subsequent discussion applies strictly only in $P-T$ regions that do not include a solvus for the fluid

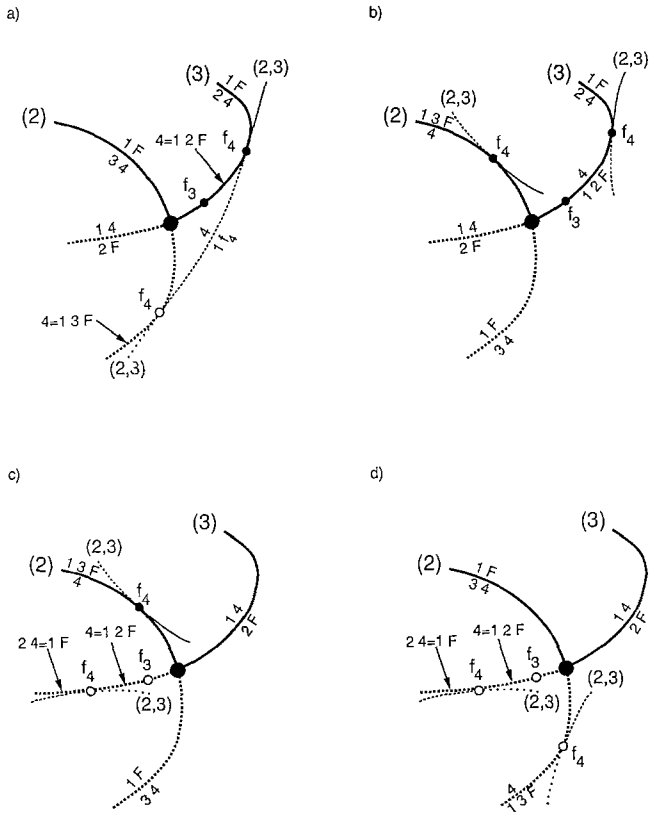

Fig. 3a–d. Choices for the location of the f_4 singular point around the invariant point illustrated in **Fig. 1b**. Singular points are labeled by the fluid phase composition (see **Fig. 1a**). On (3), the f_3 singular point must occur between the invariant point and f_4, and on (2) the f_2 singular point, which is not shown, must occur on the opposite side of the invariant point from f_4: **a** $X^{F}_{CO_2}$ increases on the stable and metastable portions of (2) and (3), respectively; **b** $X^{F}_{CO_2}$ increases on the stable extensions of (2) and (3); **c** inverse of **a**; **d** inverse of **b**. With the univariant curves as drawn, the (2, 3) singular curve can connect the f_4 singular points only for choice **a**; however, the (2, 3) curve can be made to connect the f_4 singular points if (2) and (3) cross indifferently

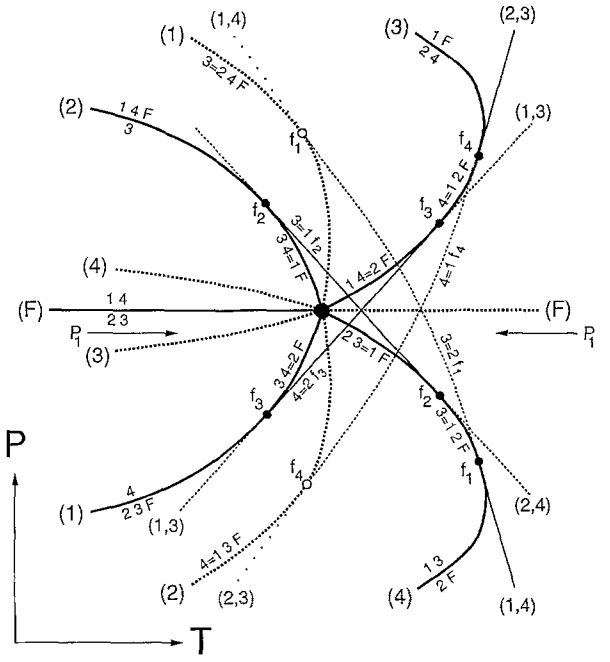

Fig. 4. Topology of the Schreinemakers projection of univariant curves and singular points around the invariant $P-T$ condition of the three-component system illustrated in **Fig. 1**. The orientation of the topology with respect to the $P-T$ axes and shapes of the curves are arbitrary. Doubly-metastable singular curves are drawn *dotted*, other line patterns and labeling as in **Fig. 2**. *Arrows* locate the $T-X^{F}_{CO_2}$ section of **Fig. 5**

a subsequent paper (R. Abart, J.A.D. Connolly, V. Trommsdorff, submitted). Referring to the system illustrated by Fig. 1a, there are only four singular equilibria, and thus several possible arrangements of the singular points. To limit discussion here to the construction of a unique arrangement, the arbitrary restriction that the topology involves no indifferent crossings of non-degenerate univariant curves will be imposed.

Given the aforementioned restriction, consider the location of the (2, 3) singular points at fluid composition f_4 along curves (2) and (3) of the invariant-point topology in Fig. 1b. Without topologic restrictions there are four choices, illustrated by the corresponding diagrams in Fig. 3: (a) $X^{F}_{CO_2}$ increases along the stable and metastable extensions of (2) and (3), respectively; (b) $X^{F}_{CO_2}$ increases along both stable extensions; (c) the inverse of (a); and (d) the inverse of (b). For choice (a) is it possible to connect the non-degenerate univariant curves by the (2, 3) singular curve without violating Schreinemakers principles. Choice (c) is not possible under any circumstance, because it requires that the singular curve crosses itself, and choices (b) and (d) are only possible if (2) and (3) cross indifferently. Thus, the f_4 singular points must occur on the stable and metastable extensions of (2) and (3), respectively, if the invariant-point topology of Fig. 1b is to be drawn without indifferent crossings. This, in turn, requires that the f_2 singular point occurs on the metastable extension of (2) and that the f_3 singular point occurs on the the stable extension of (3). Such analysis can be used to demonstrate that the topology shown in Fig. 4, or its enantiomorph, are the only topologies without indifferent crossings possible for an invariant condition with $X^{F}_{CO_2}$ between f_2 and f_3.

Relation of $P-T$ and $T-X^{F}_{CO_2}$ diagrams

The relation between the $P-T$ projection of Fig. 4 and the more common $T-X^{F}_{CO_2}$ section is illustrated by Fig. 5, which shows an isobaric section of the fluid-saturated phase relations in the $P-T$ projection at pressure P_1. This relationship can be understood if it is noted that $c+1$ phase fluid-present univariant curves in $P-T$ projection correspond to invariant points in an isobaric $T-X^{F}_{CO_2}$ section, and that $P-T$ singular curves locate thermal extrema, invariably maxima, in univariant $T-X^{F}_{CO_2}$ curves. Such extrema are designated here *extremum points*.

The $T-X^{F}_{CO_2}$ section of Fig. 5 can be reconstructed by observing that with increasing temperature along the

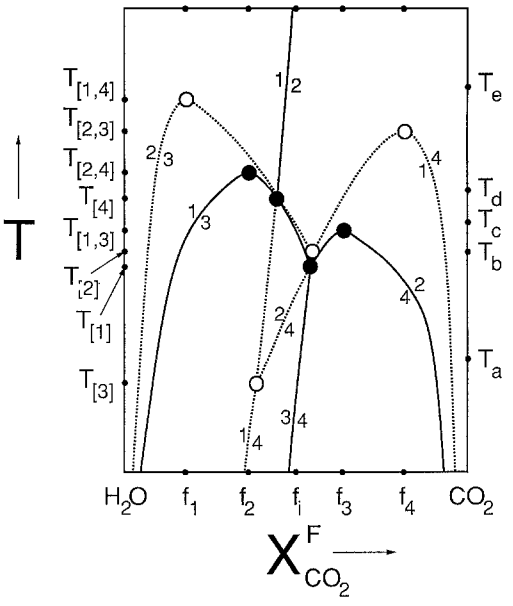

Fig. 5. $T-X^{F}_{CO_2}$ section of the phase-diagram projection shown in **Fig. 2** at pressure P_1. Labeling as in **Fig. 4**. The temperature coordinates of the composition phase diagrams a–e in **Fig. 6** are indicated along the *right* axis

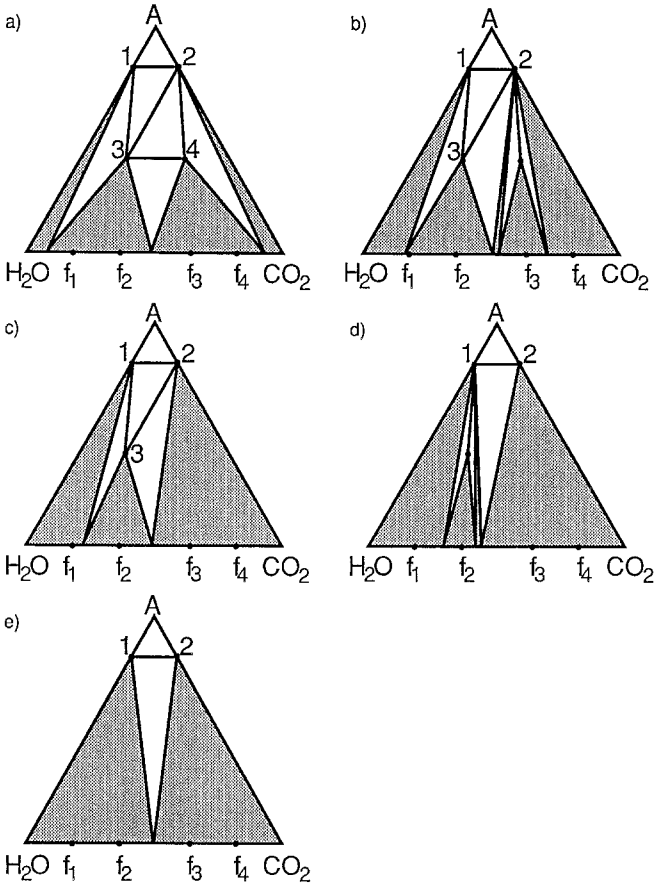

Fig. 6 a–e. Isobaric-isothermal composition phase diagrams for the system illustrated in **Figs. 1, 4, 5**. The phase diagrams are constructed at pressure P_1 (**Fig. 4**), and at temperatures shown along the *right* axis of **Fig. 5**. Two-phase regions are indicated by shading

P_1 isobar (Fig. 4), the first univariant curve intersected is the metastable portion of (3). The conditions of this intersection locate the metastable [3] invariant point in Fig. 5. The fluid composition for (3) at this intersection must lie at lower $X^{F}_{CO_2}$ than the $P-T$ invariant point composition f_i (Fig. 1a), but is otherwise unconstrained. With increasing temperature, the next curves intersected are the stable extension of (1) and the metastable extension of (2), which locate the $T-X^{F}_{CO_2}$ invariant points [1] and [2]. In the $T-X^{F}_{CO_2}$ diagram, the $X^{F}_{CO_2}$ coordinate of stable invariant point [1] is constrained between f_i and f_3, and that of metastable invariant point [2] is constrained between f_i and f_4. With an additional temperature increase, the $P-T$ singular curve (1, 3) is crossed next, which locates the stable extremum point [1, 3] at $X^{F}_{CO_2}=f_3$ in the $T-X^{F}_{CO_2}$ section, and corresponds to the maximum thermal stability of the $T-X^{F}_{CO_2}$ curve (1, 3). The next four curves along the P_1 isobar of Fig. 4 locate the stable invariant point [4] between f_2 and f_i, the stable extremum point [2, 4] at f_2, and the metastable extremum points [2, 3] at f_4 and [1, 4] at f_1. Together, these points completely define the topology of the univariant curves in the $T-X^{F}_{CO_2}$ projection illustrated by Fig. 5. It is noteworthy, that although some geometric features of the $T-X^{F}_{CO_2}$ projection cannot be determined from the $P-T$ projection, the locations of the extremum points provide quantitative constraints on many aspects of these features.

Relation of $P-T$ and composition diagrams

For further clarification of Fig. 4, a series of composition phase diagrams constructed for conditions along the P_1 isobar of Figs. 4 and 5 is shown in Fig. 6. The temperature for each composition phase diagram has been chosen, as indicated on Fig. 5, so that every diagram represents a different region of Fig. 4. Each three-phase field involving fluid in these chemographies corresponds to a point on one of the stable univariant curves in the $T-X^{F}_{CO_2}$ section of Fig. 5. For example, the assemblage 2+4 in Fig. 6b may coexist with a fluid with one of two compositions, these two compositions are the $X^{F}_{CO_2}$ ordinates of the univariant curve (1, 3) at T_b (reaction 2=4 in Fig. 5). If the chemography of Fig. 6b were redrawn at a higher temperature, but below $T_{[1,3]}$, the two fluids that may coexist with the assemblage 2+4 would approach f_3, finally degenerating completely at the [1, 3] extremum point; above this temperature the phase 4 becomes metastable (Fig. 6c). Figure 6 also shows that there are two fluid-absent assemblages, 1+2+3 and 2+3+4, which are possible for the system, but which cannot appear in the isobaric $T-X^{F}_{CO_2}$ section. These assemblages are important, because their existence precludes the stability of any assemblages involving both phases 1 and 4 in $T-X^{F}_{CO_2}$ sections at pressures below that of the invariant condition of Fig. 4. This inference would be impossible to make from a $T-X^{F}_{CO_2}$ section alone, but is clear from the fluid-absent curve (F) of the $P-T$ projection (Fig. 4), and demonstrates the importance of fluid-absent reactions in determining petrogen-

etic grids of mixed-volatile systems (Skippen and Trommsdorff 1975).

Effect of degenerate fluid compositions

The singular compositions of the fluid in the $P-T$ projection shown in Fig. 4 are non-degenerate (i.e. two-component) because the phases which decompose by the singular reactions release both components of the fluid. The singular equilibria therefore locate maxima in isobaric $T-X^{F}_{CO_2}$ sections at $0<X^{F}_{CO_2}<1$. However, frequently a phase or assemblage contains only one component of the fluid phase, i.e., as in the decomposition of hydrate or carbonate compounds. In this case, the singular $P-T$ curves locate extrema in the univariant curves of $T-X^{F}_{CO_2}$ sections at $X^{F}_{CO_2}=0$ or $X^{F}_{CO_2}=1$. To illustrate this, a $P-T$ projection for another hypothetical $A-H_2O-CO_2$ system is shown in Fig. 7. In this system, phase 1 consists of pure A; phases 2, 3, and 4, are, respectively, hydrate, carbonate, and hydrocarbonate compounds; and the fluid phase has the composition f_i at the invariant $P-T$ condition, as shown by the chemography in the inset of Fig. 7. For this chemography, there are five singular fluid compositions, of which f_1 and f_5 correspond to pure H_2O and CO_2. There are three notable differences in the phase relations of this system as compared to those of the system shown in Figs. 1 and 4: (i) the singular curves (2, 4) and (3, 4) must always be stable, and therefore are stable on both sides of the f_1 and f_5 singular conditions; (ii) the univariant curves (2), (3), and (4) all degenerate into singular curves; (iii) the phase chemography requires a minimum of one indifferent crossing of the non-degenerate univariant curves.

General implications of $P-T$ projections

The phase diagram projections shown in Figs. 4 and 7 have been oriented with respect to the $P-T$ coordinate frame by the rationale that, in general, fluid is liberated by chemical reactions with increasing temperature. As exceptions to this generality are possible, the orientation of the projection is arbitrary, though reasonable. In alternative orientations, such as when the axes are interchanged, the singular curves could represent minima in the thermal stability of phases. Another consequence of altering the $P-T$ orientation of the projection is that it might then be possible to construct an isobaric section such that the same univariant curve is intersected twice. As such intersections define invariant points in $T-X^{F}_{CO_2}$ sections, a double intersection requires that an invariant point is duplicated. Conversely, duplication of invariant points in isobaric $T-X^{F}_{CO_2}$ projections (Skippen 1971; Trommsdorff 1972) implies that the Clapeyron slope of a mixed-volatile univariant curve varies through zero.

Inspection of the stability curves depicted in Fig. 4 demonstrates the utility of $P-T$ projections for mixed-volatile systems. For example, the stability field of the assemblage $2+3$ is bounded by the curves (F), (4), and (1, 4), but in the presence of fluid, $2+3$ can exist only within the region bounded by the curves (1), (4), and

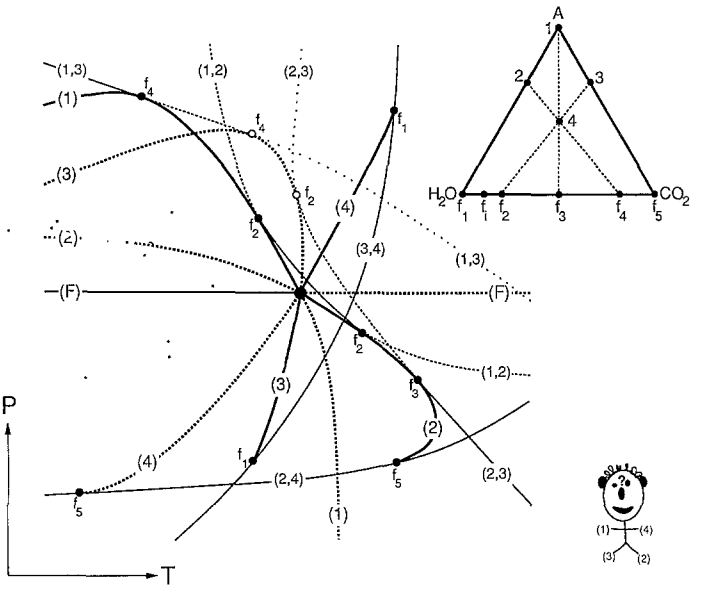

Fig. 7. An alternative chemography for the system $A-H_2O-CO_2$ (*inset*), and the resulting topology of the Schreinemakers projection of univariant curves and singular points around the invariant condition. Labeling and notation as in **Figs. 1** and **4**. Note: the singular point labeled f_2 on curve (3) should be labeled f_3

(1, 4). Another interesting aspect of the projections is that they define the absolute stability of any phase whose composition can be expressed as a positive linear combination of the possible compositions of other phases in the system, i.e. phases 3 and 4 in Fig. 4, and phases 2, 3, and 4 in Fig. 7. Most importantly, every geometric element of the $P-T$ projections can be mapped in the field. This is not always the case for isobaric $T-X^{F}_{CO_2}$ sections as discussed by Skippen (1974), who observed that in general only the unique points of $T-X^{F}_{CO_2}$ sections can be bracketed unambiguously by field mapping. All the points listed by Skippen are shown by $P-T$ projections with the exception of $T-X^{F}_{CO_2}$ indifferent crossings which are useful if different lithologies can be compared.

The foregoing discussion has been intended to illustrate the relationship between $P-T$ and $T-X^{F}_{CO_2}$ diagrams, but it has also shown that the topologic constraints on singular points provide information about the possible compositional variations of phases. This information is potentially useful for phase-diagram problems. For example, given an initial $T-X^{F}_{CO_2}$ multisystem topology these constraints can be used to predict the new multisystem topologies which could arise through changes in pressure. This paper has focused on the relations among the geologically important variables P, T, and $X^{F}_{CO_2}$. However, the same analysis could be made for any choice of solution phase, potentials, or compositional variables. Although not demonstrated here explicitly, the analysis of singular-point topology can, in general, be used to determine one compositonal variation of phase within each of the univariant equilibria related to an invariant condition. For systems containing multicomponent solutions, or more than one solution phase, each independent compositional variation of a phase in-

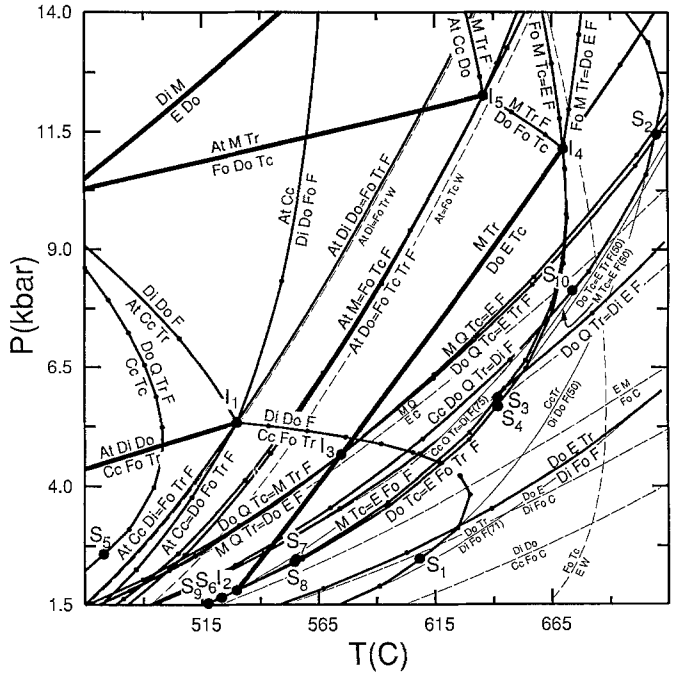

Fig. 8. Calculated $P-T$ projection for the system $CaO-MgO-SiO_2-H_2O-CO_2$ with the minerals At, Cc, Do, Di, En, M, Q, Tc, and Tr; some of the phase relations that are metastable with respect to minerals not considered in the calculation. *Thick* and *thin* curves correspond to fluid-absent and singular univariant curves, respectively; curves of *intermediate weight* locate non-degenerate fluid-present univariant equilibria; and single-volatile component singular curves are *dashed*. *Small filled circles* along univariant curves define the conditions of pseudoinvariant points as discussed in the Appendix. The approximate fluid compositions (mol% CO_2) at the invariant and singular points are: $I_1=1.0$, $I_2=86.4$, $I_3=91.2$, $I_4=5.6$, $I_5=2.3$, S_1–$S_5=50.0$, $S_6=90.0$, $S_7=83.3$, $S_8=83.3$, $S_9=90.0$, and $S_{10}=75$. Curves are labeled by the appropriate reaction equation, when the label is written on one side of the curve the high-temperature assemblage is written to the *right* of the equals sign. Note that reaction equations of the univariant curves (i.e., products or reactants) change at the singular points. The singular curves which extend from S_5 (Q-absent, see *inset* **Fig. 10a**), S_6 (E-absent, see *inset* **Fig. 10c**), S_7 (Fo-absent), S_8 (Fo-absent), and S_9 (Tc-absent) cannot be seen because they extend to low pressure and essentially overlap with other univariant curves

troduces at least one degree of freedom in the analysis. In such cases, empirical information is necessary to select the relevant topology.

A $P-T$ projection for the system $CaO-MgO-SiO_2-H_2O-CO_2$

The system $CaO-MgO-SiO_2-H_2O-CO_2$ is critical for understanding the phase relations of many carbonate-bearing rocks and will be used here to demonstrate the geologic application of $P-T$ projections for a mixed-volatile system. The $P-T$ projection for this system, shown in Fig. 8, was calculated considering the phases At, Cc, Do, Di, En, M, Q, Tc, Tr, and fluid (see Table 1 for notation) with the data of Berman (1988), Kerrick and Jacobs (1981), and J.A.D. Connolly V. Trommsdorff, R. Philipp (in revision). With regard to the geologic significance of this projection, it should be observed that: (i) some of the high-temperature phase relations are metastable with respect to amphibole assemblages; (ii) phase relations involving wollastonite, periclase, and brucite are not shown; and (iii) the high-pressure stability field of talc may be larger than that predicted from the thermodynamic data.

In Fig. 8 thick, intermediate, and thin solid curves represent, respectively, fluid-absent, fluid-present, and mixed-volatile singular univariant equilibria; and the thin dashed curves correspond to dehydration or decarbonation singular equilibria. It is noteworthy that magnesite occurs along three fluid-absent univariant curves with distinct Clapeyron slopes in Fig. 8; this accounts for the extreme sensitivity of $CaO-MgO-SiO_2-T-X^F_{CO_2}$ diagram topologies to the thermodynamic properties of magnesite as discussed by Trommsdorff and Connolly (1990).

The most striking feature of the phase-diagram projection shown in Fig. 8 is that the variation in Clapeyron slopes, both along individual univariant curves and among different curves, is much stronger than in fixed-fluid composition projections. The projections are therefore useful as petrogenetic grids because the univariant curves dissect $P-T$ space into relatively restricted regions. To demonstrate this, the stability fields of individual phase assemblages within the $P-T$ projection of Fig. 8 are shown in Fig. 9 and discussed in the following paragraphs. In Fig. 9 the approximate composition of the fluid in univariant assemblages is indicated at intervals along each curve, fluid compositions are not shown in Fig. 8 to avoid cluttering the diagram.

Comparison of the $P-T$ diagrams of Figs. 8 and 9 with the $T-X^F_{CO_2}$ and $P-X^F_{CO_2}$ sections shown in Fig. 10 reveals small discrepancies in the $P-T-X^F_{CO_2}$ coordinates of the phase elements. These discrepancies occur because the $P-T$ diagrams have been calculated using an approximation discussed in the appendix, whereas the calculations of the $T-X^F_{CO_2}$ and $P-X^F_{CO_2}$ sections were numerically exact.

Cc + Tc assemblage

The stability field of the assemblage Cc + Tc, limited by the univariant curve Cc + Do + Q + Tc + Tr + F, is presented in Fig. 9a. In isobaric $T-X^F_{CO_2}$ section the Cc + Do + Q + Tc + Tr + F curve corresponds to an invariant point which defines the upper $T-X^F_{CO_2}$ limits of the Cc + Tc stability field as shown by Fig. 10a. The pressure dependence of this $T-X^F_{CO_2}$ stability field has been the subject of some dispute (Skippen 1974; cf. Slaughter et al. 1975) and the backbending character of the Cc + Do + Q + Tc + Tr + F curve in Fig. 9a suggests a diplomatic solution, at least in $P-T$ space; namely that the thermal stability of Cc + Tc increases with pressure reaching a maximum at about 5 kbar, thereafter it decreases with pressure (see also Evans and Guggenheim 1988). From the fluid composition along the Cc + Do + Q + Tc + Tr + F curve it can be determined that the range of fluid compositions over which the assemblage Cc + Tc is stable decreases continuously with

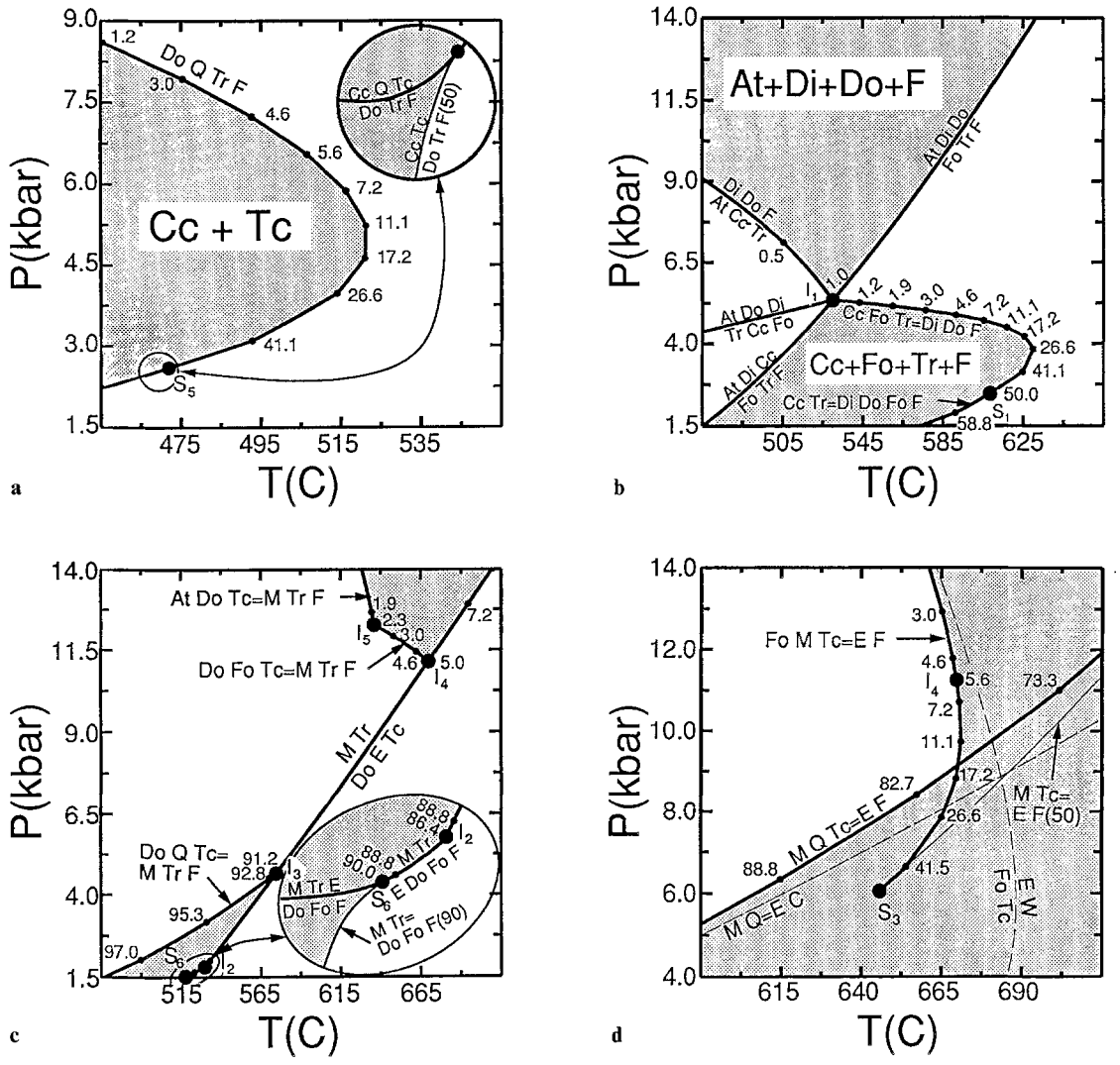

Fig. 9a–d. Stability fields in the $P-T$ projection of **Fig. 8**: **a** Cc+Tc; **b** Cc+Fo+Tr and Di+Do+Ant; **c** M+Tr; **d** E+F. Fluid-saturated fields are indicated by *shading*. Reduction in fluid pressure (i.e., $P_{fluid} < P_{total}$) would expand the fluid-present fields of: **b** Fo+Tr+Cc; **c** M+Tr; **d** E; would reduce the field of **a** Cc+Tc, and displace the field toward lower temperature and pressure. *Insets* show details around **a** S_5 Q-absent singular point and **c** S_6 E-absent singular point. In **d** the fluid-saturated stability field of E is limited by two different eutectoidal reactions at $P > P_{S_3}$. For fluids with $X^F_{CO_2} > 50$ mol% the limiting reaction is M+Q+Tc=E, and for H_2O-rich fluids the reaction is M+Fo+Tc=E. The (*heavy solid*) curves corresponding to these reactions are connected by the singular (*thin solid*) curve for the Q+Fo-absent reaction M+Tc=E+F(50) in $P-T$ space, and separated by this reaction in $X^F_{CO_2}$ space (see **Fig. 10a**)

pressure. At pressures below S_5 ($X^F = 0.5$), the Q-absent singular point, the Cc+Do+Q+Tc+Tr+F curve no longer limits the stability of assemblage Cc+Tc, which is instead limited by the singular curve for the equilibrium Cc+Tc=Do+Tr+F ($X^F_{CO_2} = 0.5$) (inset Fig. 9a). This implies that in $T-X^F_{CO_2}$ sections at $P < P_{S_5}$ the maximum thermal stability of Cc+Tc assemblages is limited by an extremum point rather than an invariant point.

Cc+Fo+Tr and At+Di+Do assemblages

The fact that the Clapeyron slopes of many fluid-absent reactions are near zero causes the stability of many mineral assemblages to be limited by $P-T$ invariant points. The fluid-absent curve At+Cc+Di+Do+Fo+Tr which emanates from invariant point I_1 (Fig. 8) provides a geologically important example of this. This curve dissects $P-T$ space into two regions which limit the stability of Cc+Fo+Tr and At+Di+Do assemblages to, respectively, low and high pressures. Although these assemblages may coexist stably along the entire length of the At+Cc+Di+Do+Fo+Tr curve, they only may coexist together with a fluid phase at invariant point I_1. Invariant point I_1 thus defines the minimum and maximum pressure for stability of the fluid-saturated assemblages as shown by Fig. 9b. The mutually exclusive pressure stability fields for Cc+Fo+Tr and At+Di+Do assemblages is consistent with: (i) the common occurrence of Cc+Fo+Tr assemblages in contact aureoles (Moore and Kerrick 1975; Rice 1977) and its relative rarity in regionally metamorphosed rocks (Tromms-

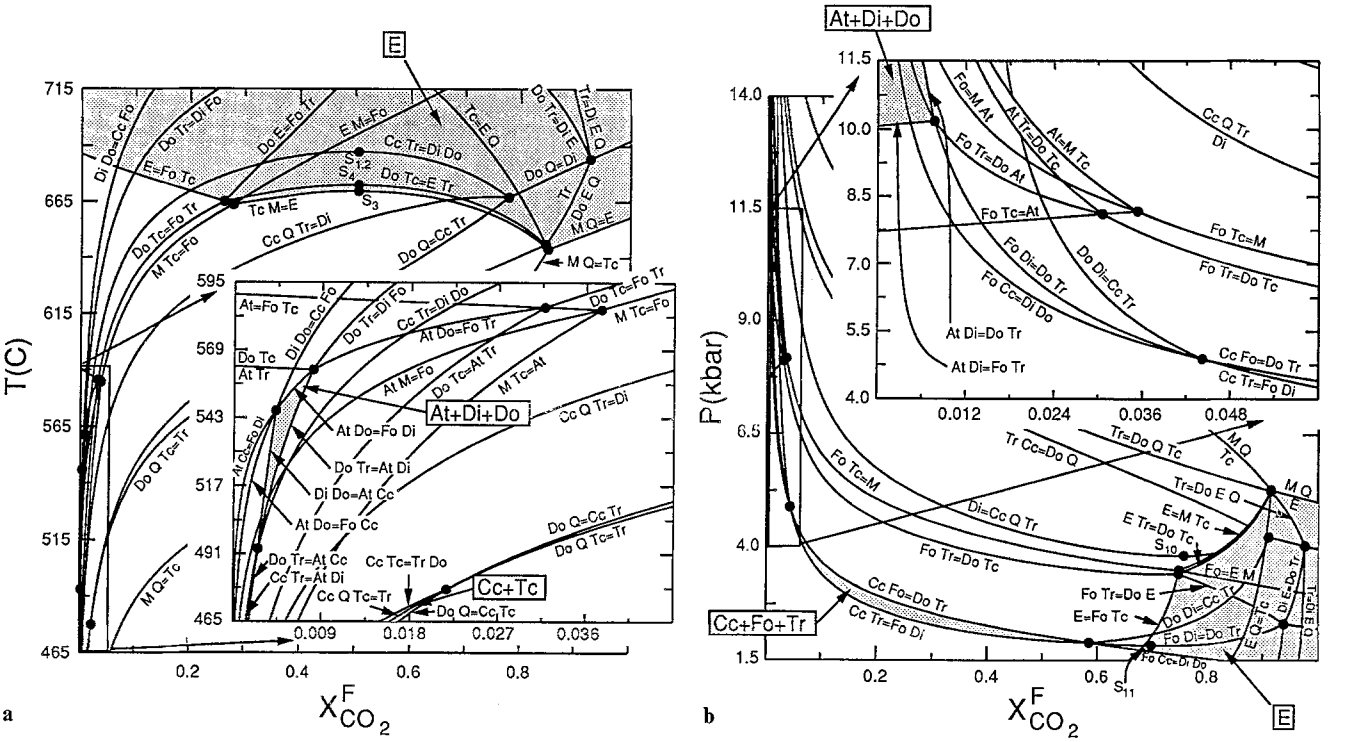

Fig. 10a, b. Sections of **Fig. 8: a** isobaric ($P=7.75$ kbar) $T-X^F_{CO_2}$; **b** isothermal ($T=580°$ C) $P-X^F_{CO_2}$. *Insets* show details of the H_2O-rich regions of the diagrams. Reaction equations are written with the high-temperature assemblage on the *right* side of the equals sign in **a** and with the high-pressure assemblage on the *right* in **b**. *Shaded* regions are the stability fields of E (**a** and **b**), At + Di + Do (*insets* of **a** and **b**), Cc + Tc (*inset* of **a**), and Cc + Fo + Tr (**b**). The stability field of Cc + Fo + Tr is limited by duplicate invariant assemblages

dorff 1972); (ii) the restriction of At + Di + Do to high-pressure ophicarbonate rocks (Trommsdorff and Evans 1977b).

Invariant points in $P-T$ projections may also define thermal extrema in the stability of a mixed-volatile assemblage. For example, I_1 (Fig. 8) defines the maximum and minimum thermal stability, respectively, of the assemblages At + Cc + Tr and Di + Do + Fo + F.

A point of academic interest in Fig. 8 is that many of the univariant phase curves have Clapeyron slopes that vary through infinity. As a result the duplication of invariant points in $P-X^F_{CO_2}$ sections is relatively commonplace. An example of this is provided by the univariant curve Fo + Tr + Cc + Di + Do + F (see also Fig. 9b), which appears as two invariant points limiting the stability of Fo + Tr + Cc in the $P-X^F_{CO_2}$ section of Fig. 10b. There is no univariant curve in Fig. 8 for which the Clapeyron slope changes sign through zero, consequently duplication of invariant points does not occur in any isobaric $T-X^F_{CO_2}$ section through the $P-T$ projection.

M + Tr assemblage

The assemblage M + Tr + F is an example of an assemblage with two very distinct stability fields depending on fluid composition (Fig. 9c). At high pressures, above I_4, assemblage M + Tr is stable with H_2O-rich fluids (this is borne out by its occurrence in sagvandites: Schreyer et al. 1972; Pfeifer 1979; Evans and Trommsdorff 1983; Bucher-Nurminen 1988), whereas at low pressure, below I_3, the assemblage may form in CO_2-rich fluids. It is noteworthy that because the fluid-absent equilibrium M + Tr = E + Do + Tc is compositionally degenerate it may occur in the presence of a fluid at pressures above I_4 and below I_3.

E + F assemblage

The fluid-saturated stability field of enstatite (Fig. 9d) is delimited by five univariant curves some of which intersect at indifferent crossings. This may at first seem to contradict Schreinemakers rules, but is a common feature of projections for systems with phases of variable composition (Schreinemakers 1917). The explanation for this behavior is that the low-temperature limit of any phase, or phase assemblage, is defined by either a eutectoid or singular reaction. If a phase in an assemblage has variable composition then there may be several different eutectoids and singular reactions depending on the composition of this phase. The equilibrium conditions for each of these reactions define a univariant curve in $P-T$ projection, but as only one of these reactions is possible for a system with fixed bulk composition these curves cross only at indifferent conditions. Each eutectoid must be separated from the other eutectoids in composition space by singular reactions; thus, in the

case of E+F at pressures above the Q+Fo-absent S_3 singular point in Fig. 9d, the eutectoidal reactions[4] E+F=M+Q+Tc and E+F=M+Fo+Tc (heavy solid curves) are separated in composition space by the singular reaction E+F(50)=M+Tc (thin solid curve), and flanked by the singular reactions $E+CO_2=M+Q$ and $E+H_2O=Fo+Tc$ (dashed curves), this can be seen clearly in Fig. 10a. At singular point S_3 (Fig. 9d), the reaction equation of the M+Fo+Tc+E+F curve becomes peritectoidal (i.e., M+Tc=E+Fo+F) and no longer limits the stability of E+F. Extrapolation of the M+Q+Tc+E+F univariant curve and the E+F(50)=M+Tc singular curve to higher temperatures suggests that the E+F=M+Q+Tc eutectoid terminates at a singular point at a pressure of about 14 kbar. Likewise extrapolation of the pure-fluid singular curves indicates that in the limiting cases of extremely low and high pressure, the E+F eutectoids occur, respectively, in pure H_2O and CO_2 fluids. The points at which these singular curves become eutectoids would be analogous to the singular points f_1 and f_5 in Fig. 7.

Narrow divariant fields

A number of divariant and higher-variance assemblages in the $CaO-MgO-SiO_2-H_2O-CO_2$ phase diagram have such narrow $P-T$ stability fields that for practical purposes the assemblages behave as univariant $P-T-X^F_{CO_2}$ indicators. Perhaps the best example of this in Fig. 8 is the stability field of Do+E+Fo+Tc+F which is bounded by the univariant curves E+Fo+M+Tc+F and Do+E+Fo+Tc+Tr+F between I_2 ($X^F_{CO_2}=91.2$) and I_4 ($X^F_{CO_2}=5.6$). The occurrence of this assemblage, together with an independent constraint on either P, T, or $X^F_{CO_2}$ (assuming fluid-saturation), could be used to estimate the remaining metamorphic variables. Other examples of narrow high-variance phase fields in Fig. 8 are: (i) Do+E+Q+Tc+F, $P>P_{I_3}$; (ii) M+Q+Tr+F, $P<P_{I_3}$; (iii) M+Tr+Fo+F, $P<P_{I_2}$ (this field is too narrow to be seen clearly in Fig. 8, the assemblage also has a high-pressure stability field at $P>P_{I_4}$); (iv) At +Do+Fo+Tc+F, $P<P_{I_5}$; (v) At+Fo+M+Tr+F, $P>P_{I_5}$.

Discussion

The objective of this paper has been to draw attention to the utility of $P-T$ projections in the petrogenetic analysis of mixed-volatile systems. The fundamental advantage of such projections, over conventional $T-X^F$ or $P-X^F$ sections, is that the influence of both pressure and temperature is shown simultaneously. The cost of this information is that it is not practical also to show explicitly the composition of the fluid in equilibrium with high-variance mineral assemblages. This is a potential limitation in applications of $P-T$ projections to geologic systems which have been open to a fluid with externally controlled composition. However, many geologic systems are capable of controlling (i.e., buffering) the composition of fluids, and in such cases the univariant and singular curves of $P-T$ projections are the only mappable phase-diagram features. More generally, $P-T$ projections are always preferable to $T-X^F_{CO_2}$ sections for situations, such as those common in regional metamorphic studies, in which pressure cannot be estimated independently of phase equilibria. A drawback to using $P-T$ projections to represent phase relations for mixed-volatile systems has been that they are difficult to calculate. This paper also has been intended to demonstrate that existing computational methods (Connolly 1990) easily can be adapted to make feasible the calculation of $P-T$ projections from thermodynamic data.

The principles governing the topology of phase-diagram projections are usually presented without consideration of the arrangement of singular points. This is of no consequence in applications to systems in which phases have no compositional degrees of freedom (i.e., the phases are all compounds); but, in a system where one or more phases have variable composition (e.g., a mixed-volatile fluid), singular-point topology can provide useful constraints. In the case of a geologic system containing minerals of fixed composition and a binary H_2O-CO_2 fluid, such constraints can be used to determine the direction of variation in fluid composition along the univariant equilibria emanating from an invariant condition. The topologic constraints are not based on thermodynamic data and are therefore useful for predicting phase-diagram topologies or testing the consistency of $T-X^F_{CO_2}$ or $P-X^F_{CO_2}$ multisystem topologies. The same analysis can be used to predict the behavior of any system containing one or more solution phases.

Appendix: calculation of $P-T$ projections for mixed-volatile systems

Calculations of $P-T$ projections for a system with a mixed volatile of variable composition are considerably more complicated than those for systems with phases without compositional degrees of freedom. The complication arises because it is not only necessary to determine the $P-T$ conditions of equilibria, but also the equilibrium compositions of the fluid, which, for practical purposes, can only be accomplished by computerized numerical free-energy minimization[5]. Unfortunately, the only procedure which couples numerically exact energy minimization with an algorithm for the calculation of $P-T$ projections (Holland and Powell 1990) cannot at present be used for non-ideal solution models such as those commonly used to describe fluids. As an alternative to numerically exact minimization procedures, the

[4] Strictly these reactions are only eutectoidal for fluid-saturated systems.

[5] Trommsdorff and Evans (1977b) and Carmichael (1991) have calculated univariant $P-T$ equilibria by iteratively locating the corresponding isobaric $T-X^F_{CO_2}$ invariant points. This approach is time consuming and difficult to integrate into a strategy for phase-diagram calculation; moreover, it is unsuitable for systems in which phases other than the fluid have variable composition.

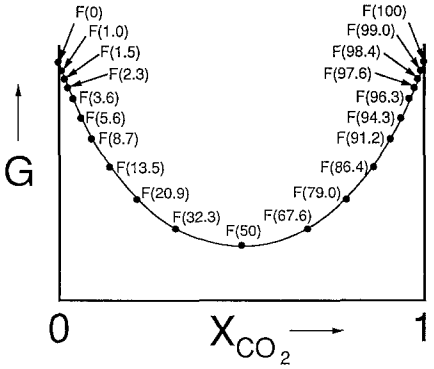

Fig. 11. Schematic free energy(G)-composition diagram illustrating the compositions of the pseudocompounds used to represent the fluid phase in **Figs. 8** and **9**. The logarithmic spacing of the pseudocompounds provides better resolution of fluid composition near the extremes of $X^F_{CO_2}$

calculations for this study were done using the "pseudocompound approximation" of Connolly and Kerrick (1987) which is implemented in the Vertex computer program (Connolly 1990). The purpose of this appendix is to provide the reader with a basis for understanding the output from Vertex which consists of diagrams and lists of the stable phase equilibria defined in terms of pseudocompounds. An advantage of Vertex is that it can be used to calculate equilibria in systems with mineral solutions as well as a fluid.

With the pseudocompound approximation a set of arbitrarily defined compounds, i.e., *pseudocompounds*, are used to represent the possible compositions of the fluid. A simple linear optimization procedure can then be used to determine the stability of the pseudocompounds and thereby the approximate equilibrium composition of the solution represented by them. As a result of this approximation the continuous compositional variation of a solution phase is represented by a series of discrete steps. For example, in the phase-diagram calculations presented here, H_2O-CO_2 fluids were represented by 23 pseudocompounds with a logarithmic compositional spacing that is symmetrical about $X^F_{CO_2}=0.5$ as illustrated by Fig. 11. It is to be noted that the shape of the $G-X$ curves used by Vertex is not prescribed; thus, the program can be used for fluids which have solvii.

A $P-T$ univariant curve, calculated by Vertex, is then defined by a series of segments along each of which one fluid pseudocompound is stable and the reaction equation has constant coefficients. These segments may intersect at two different types of points: (i) true invariant points at which $c+1$ minerals and one fluid pseudocompound coexist; (ii) *pseudoinvariant points* at which c minerals and two fluid pseudocompounds coexist. Pseudoinvariant points are the conditions at which one fluid pseudocompound becomes metastable with respect to another; such a condition thus approximates the continuous variation of fluid composition by a discrete step along the univariant $P-T$ curve. The magnitude of these steps, and thereby the compositional resolution of calculations, is dictated by the compositional spacing of the pseudocompounds specified by the user of Vertex. The logarithmic subdivision scheme illustrated in Fig. 11 results in resolution on the order of $\pm 0.5\%$ at the extremes of $X^F_{CO_2}$, and of $\pm 9\%$ at $X^F_{CO_2}=50.0$ mol% CO_2. In Figs. 8 and 9 the small dots along the univariant curves locate pseudounivariant conditions, and in Fig. 9 the fluid compositions have been estimated by averaging the composition of the coexisting pseudocompounds.

As the number of pseudocompounds plus compounds must be $c+2$ at any pseudoinvariant point, $c+2$ univariant curves must emanate from each pseudoinvariant point. Of these, two must define equilibria involving c minerals and one fluid pseudocompound and correspond to a real univariant $c+1$-phase equilibrium. The remaining c univariant curves, designated *pseudounivariant curves*, define equilibria involving c-1 minerals and two fluid pseudocompounds. These pseudounivariant curves are, in essence, fluid isopleths of the divariant phase fields around each univariant curve for which the fluid composition is the average of that of the pseudocompounds.

Pseudounivariant assemblages can be recognized by Vertex, but were not computed for Figs. 8 and 9 to avoid complicating the diagrams. However, by showing pseudounivariant equilibria in $P-T$ projections it is possible to present all the information shown by conventional $T-X^F_{CO_2}$ or $P-X^F_{CO_2}$ diagrams. As an example, Fig. 12a shows the pseudounivariant curves that radiate from the pseudoinvariant points (P_1–P_5) around the I_1 invariant point of Figs. 8 and 9b at which the assemblage At+Cc+Di+Do+Tr+F(1.0) is stable. The (solid) univariant curve Cc+Di+Do+Fo+Tr+F(1.0) is stable from I_1 to pseudoinvariant point P_2 at which the assemblage Cc+Di+Do+Fo+Tr+F(1.0)+F(1.5) is stable. Point P_2 thus represents a condition at which the true fluid composition is $X^F_{CO_2}=1.25$ mol% CO_2. The stability of five divariant assemblages Cc+Di+Do+Fo+F, Cc+Di+Do+Tr+F, Cc+Di+Fo+Tr+F, Cc+Do+Fo+Tr+F, and Di+Do+Fo+Tr is limited by the univariant curve, and each of these assemblages represented by a pseudounivariant curve around P_2 involving the F(1.0) and F(1.5). Each pseudounivariant curve therefore defines the $P-T$ conditions for which the fluid composition is buffered at ca. 1.25 mol% CO_2 for the relevant divariant assemblage. As a divariant $P-T$ field corresponds to a univariant curve in $T-X^F_{CO_2}$ and $P-X^F_{CO_2}$ sections, the pseudounivariant $P-T$ curves can be used to locate univariant curves in either section as can be verified by comparison of Fig. 12 with 10.

In interpreting $P-T$ projections calculated with Vertex it is important to remember that the nominal fluid compositions for invariant and univariant equilibria involving both fluid components are always approximate. For example, the stability of the F(1.0) pseudocompounds at I_1 must be interpreted in light of the fact that the compositions considered in a calculation are predefined (Fig. 11). For the I_1 invariant point this means that the F(1.0) pseudocompound is stable with respect to the compositionally adjacent pseudocompounds, F(0) and F(1.5), but the true stable composition of the fluid could be at any intermediate value. Likewise, at pressures above those of the P_1 and P_4 pseudoinvariant points, the stability of the F(0) (i.e., H_2O) pseudocom-

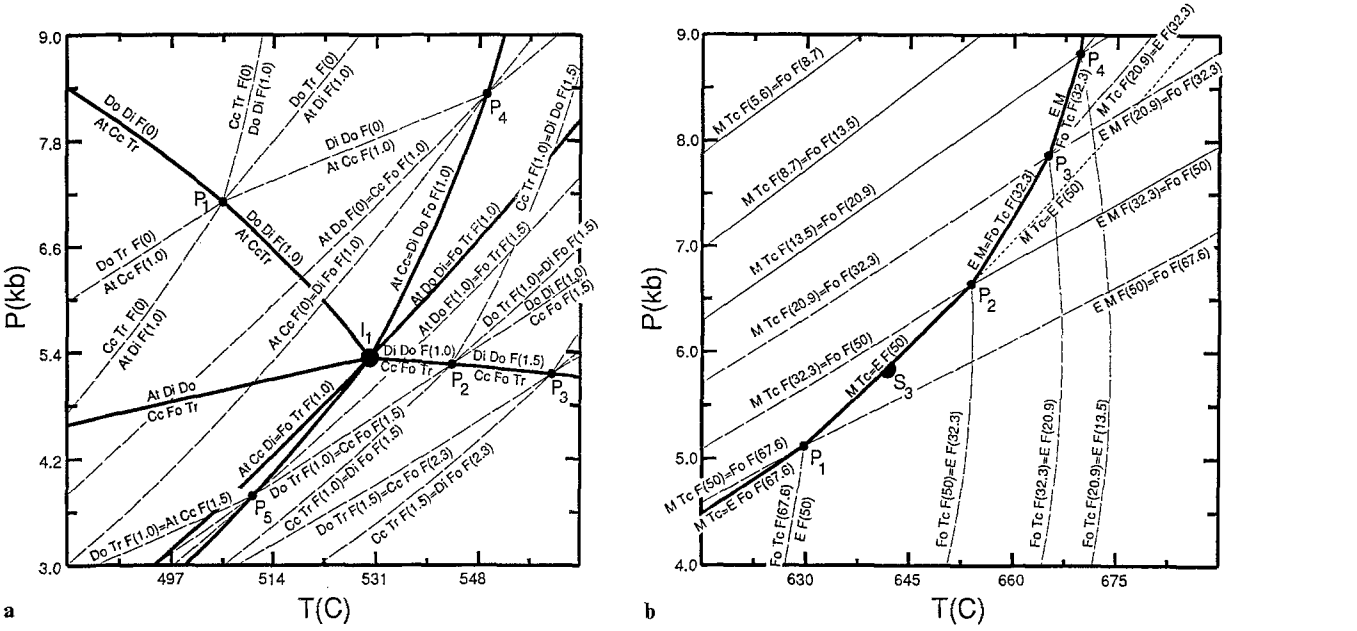

Fig. 12a, b. Details of **Fig. 8** showing phase relations around: **a** the I_1 invariant point (see also **Fig. 9b**); **b** the S_3 singular point (see also **Fig. 9d**). Univariant, singular, and pseudounivariant equilibria are represented by, respectively, *solid*, *thin solid*, and *thin dashed* curves. For simplicity only pseudoinvariant curves which emanate from the pseudoinvariant points within the coordinate frames of the diagrams are shown. The pseudocompound assemblages can be used to estimate fluid composition. For example, in **a** at pseudoinvariant point P_1, pseudocompounds F(0) and F(1.0) coexist, which implies the true composition of the fluid at this point is between pure H_2O and $X^F_{CO_2} = 1.0$ mol%. The five pseudounivariant curves which emanate from this point are isopleths for the fluid composition in the five divariant fields which meet along the univariant curve. Note that although the pseudocompound in the univariant assemblage At+Cc+Di+Do+Tr+F(0) is pure H_2O, this does not mean the equilibrium is stable in pure H_2O fluids, but rather it implies that the equilibrium is not stable in a fluid with the composition of the next most H_2O-rich pseudocompound (F(1.0))

pound is deceptive and should not be taken to imply that either of the relevant equilibria are stable in pure H_2O. Rather, the stability of the F(0) compound indicates that the next most H_2O-rich pseudocompound, F(1.0), is metastable.

A weakness of the pseudocompound approximation is that any singular curve will join a non-degenerate univariant curve along a finite segment of the univariant curve rather than at a true singular point. An example of this is the M+Tc=E+F(50) singular curve which intersects the M+Tc+E+Fo+F univariant curve of Fig. 8 at S_3. In Fig. 12b it can be seen that the singular and univariant curves overlap between pseudoinvariant points P_1 and P_2. The location of the S_3 singular point, has been taken somewhat arbitrarily as being between the pseudoinvariant points defining the tangent portion of the singular and univariant curves. A second drawback of the pseudocompound approximation is that singular equilibria will not be found directly unless a pseudocompound with the singular composition is defined (examples of this are the S_5–S_{11} singular curves of Fig. 8 which were calculated after the initial phase-diagram calculation). Although some singular curves may not be calculated by Vertex, the location of singular points always can be determined from the change in sign of a reaction coefficient along a univariant curve.

Acknowledgements. Financial support from Schweizerischer National Fonds grant 20-26223.89 is gratefully acknowledged. We are indebted to Rainer Abart who, among other things, corrected a major topological error, and to Thomas Driesner who found a labeling error. We thank Howard Day, Bernard Evans, Rainer Abart, and Martin Engi for comprehensive and constructive reviews.

References

Berman RG (1988) Internally consistent thermodynamic data for minerals in the system $Na_2O-K_2O-CaO-MgO-FeO-Fe_2O_3-SiO_2-TiO_2-H_2O-CO_2$. J Petrol 29:445–552

Bucher-Nurminen K (1988) Metamorphism of ultramafic rocks in the central Scandinavian Caledomides. Nor Geol Unders Spec Publ 3:86–95

Connolly JAD (1990) Calculation of multivariable phase diagrams: an alogrithm based on generalized thermodynamics. Am J Sci 290:666–718

Connolly JAD, Kerrick DM (1987) An algorithm and computer program for calculating computer phase diagrams. CALPHAD 11:1–55

Evans BW, Guggenheim S (1988) Talc, pyrophyllite and related minerals. (Reviews in Mineralogy 19) Mineral Soc Am, Washington, D.C., pp 225–294

Evans BW, Trommsdorff V (1983) Flourine hydroxyl titanian clinohumite in alpine recrystallized peridotite: compositional controls and petrologic significance. Am J Sci 283-A:355–369

Holland TJB, Powell R (1990) An enlarged and updated inernally consistent thermodynamic dataset with uncertainties and correlations: the system $K_2O-Na_2O-CaO-MgO-FeO-Fe_2O_3-Al_2O_3-SiO_2-C-H_2-O_2$. J Metamorphic Geol 8:89–124

Greenwood HJ (1962) Metamorphic reactions involving two volatile components. Annu Rep Dir Geophys Lab 61:82–85
Kerrick DM, Jacobs GK (1981) A modified Redlich-Kwong equation for H_2O, CO_2 mixtures at elevated pressures and temperatures. Am J Sci 281:735–767
Moore JN, Kerrick DM (1976) Equilibria in siliceous dolomites of the Alta aureole, Utah. Am J Sci 276:502–524
Pfeifer HR (1979) Fluid-Gesteins-Interaktion in metamorphen Ultramafititen der Zentralalpen. PhD Thesis ETH Zurich No. 6379
Rice JM (1977) Contact metamorphism of impure dolomitic limestone in the Boulder Aureole, Montana. Contrib Mineral Petrol 59:237–259
Schreinemakers FAH (1916) (i) Further consideration of the bivariant regions; the turning lines. Versl Koninklijke Akad Wetenscap 18:1539–1552
Schreinemakers FAH (1917) (ii) The regions in *P*, *T* diagrams. Versl Koninklijke Adad Wetenscap 19:180–187
Schreinemakers FAH (1924) (iii) Singular equilibria. Versl Koninklijke Akad Wetenscap 27:800–808
Schreyer W, Ohnmacht W, Mannchen J (1972) Carbonate orthopyroxenites (sagvandites) from Troms, Northern Norway. Lithos 5:345–364
Skippen G (1971) Experimental data for reactions in siliceous marbles. J Geol 79:457–487
Skippen GB (1974) An experimental model for low pressure metamorphism of siliceous dolomitic marble. Am J Sci 274:487–509

Note. J. Baker, T. Holland, and R. Powell have published a paper (1991, Contrib Mineral Petrol 106:170–182) on aspects of P–T projections for mixed-volatile systems which is similar to D. M. Carmichaels paper mentioned in the introduction of this paper.

Skippen GB, Trommsdorff V (1975) Invariant phase relations among minerals on $T-X_{fluid}$ sections. Am J Sci 275:561–572
Slaughter J, Kerrick DM, Wall JV (1975) Experimental and thermodynamic study of equilibria in the system $CaO-MgO-SiO_2-H_2O-CO_2$. Am J Sci 275:143–162
Trommsdorff V (1972) Change in $T-X$ during metamorphism of siliceous dolomitic tocks of the Central Alps. Schweiz Mineral Petrogr Mitt 52:1–4
Trommsdorff V, Connolly JAD (1990) Constrains on phase diagram topology for the system $CaO-MgO-SiO_2-H_2O-CO_2$. Contrib Mineral Petrol 104:1–7
Trommsdorff V, Evans BW (1977a) Antigorite-ophicarbonates: Phase relations in a portion of the system $CaO-MgO-SiO_2-H_2O-CO_2$ Contrib Mineal Petrol 60:39–56
Trommsdorff V, Evans BW (1977b) Antigorite-ophicarbonates: contact metamorphism in Valmalenco, Italy. Contrib Mineral Petrol 62:301–312
Wyllie PJ (1962) The petrogenetic model, an extension of Bowen's petrogenetic grid. Geol Mag 99:558–569
Zen E (1966) Construction of pressure-temperature diagrams after the method of Schreinemakers – a geometric approach. US Geol Surv Bull 1225

Editorial responsibility: J. Hoefs